Thermo-tectonic evolution of a convergent orogen with low topographic build-up

Merten, S.

2011

document version
Publisher's PDF, also known as Version of record

CHAPTER 5

Collisional characteristics of an orogen with low topographic build-up: Integration of the high-resolution exhumation history of the SE Carpathians at the scale of the entire Romanian Carpathians[1]

5.1 Introduction

In the evolution of convergent orogens, the moment when the thinned continental crust carried by the lower plate reaches the subduction zone is generally considered as the onset of continental collision. First order observations regarding orogenic collision are provided by dating deformations along the frontal sole thrust, which marks the end of deformation in a normal, foreland-breaking sequence of thrusting. Furthermore, field and numerical modelling studies have demonstrated that continental collision coincides with the onset of large-scale out-of-sequence deformation [e.g. *Willett and Brandon*, 2002]. This is most commonly expressed by concentrated exhumation along step-up hinterland vergent retro-shears (i.e. crustal-scale backthrusts), where the upper-plate exhumation is enhanced by denudation [e.g. *Beaumont et al.*, 1994]. One structural example described as typical for such retro-shears is the Insubric Line in the European Alps [*Schmid et al.*, 1996]. In these type of orogens, exhumational steady-state is characterised by reset thermochronological ages spatially nested against the retro-deformation front [e.g. *Willett and Brandon*, 2002]. However, collisional coupling (i.e. far-field transmission of compressional orogenic stresses) has been

[1]This chapter is partly based on: Matenco, L., Krézsek, C., Merten, S., Schmid, S., Cloetingh, S., Andriessen, P., 2010. Characteristics of collisional orogens with low topographic build-up: an example from the Carpathians. *Terra Nova, 22*, 155–165.

documented to be responsible for intra-plate compressional deformation in orogenic forelands [*Ziegler et al.*, 1995]. This observed feature of strain partitioning in the lower (subducting) plate during collision is generally ignored by existing geodynamic models.

Retro-shears are less obvious in orogens that are characterised by "soft"-collision i.e. where low amounts of bulk exhumation are recorded by thermochronological studies. This is often observed in highly arcuate thrust belts, which are associated with back-arc extension in the overriding plate and rates of subduction that are higher than plate convergence rates [e.g. *Faccenna et al.*, 2004]. Collision, if present, is generally defined as being early or incomplete in comparison to orogens considered to have reached steady-state equilibrium [e.g. *Royden*, 1993]. The formation of this type of mountain chains has been explained in terms of age of the subducted oceanic lithosphere, slab-pull, rates of convergence between plates [*Royden and Burchfiel*, 1989], or in terms of the geographic direction of subduction [*Doglioni et al.*, 1999]. Monitoring mountain building during collision of such orogens is generally hampered by low amounts of exhumation. Temperatures reached by exhumed rocks are likely to be near or even below the closure temperatures of most thermochronometers. Exhumation pathways may be affected by lateral transport inside the orogen and longer residence in partial retention zones, and thermochronometers tend to reflect the cumulative exhumation of multiple tectonic episodes [*Reiners and Brandon*, 2006]. "Soft"-collision, exhumation of the orogenic core in the absence of retro-shears, formation of back-arc basins and/or exhumation resulting from syn-orogenic extension are common in Mediterranean-type mountain belts, which are difficult to explain by the simple retro-shear model (e.g. Apennines, Dinarides, Calabria, Betics, Hellenides) [e.g. *Jolivet and Faccenna*, 2000; *Brun and Faccenna*, 2008].

The low-topography Carpathian orogen (Figure 5.1) is a case where crustal-scale backthrusting in the orogenic core, although postulated on indirect grounds at the contact with the Transylvania back-arc basin [*Sanders*, 1998], has never been confirmed [*Krézsek and Bally*, 2006]. This uncertainty raises the question as to whether collision is accompanied by backthrusting or not. Because of low amounts of exhumation during and after collision, the post-tectonic cover is still present, allowing biostratigraphic dating of nappe-stacking events and discrimination from stages of post-collisional deformation [*Matenco et al.*, 2007]. Low-temperature thermochronology was used to derive a detailed exhumation history for the SE Carpathians (Figure 5.1), describing the evolution from the Late Cretaceous and Miocene nappe-stacking events to the Quaternary post-collisional deformations (see Chapter 4). In order to integrate this high-resolution exhumation history into the general evolution of the Romanian Carpathians, samples from the East and South Carpathians dated for apatite fission track (AFT) thermochronology by *Sanders* [1998] and *Sanders et al.* [1999] were reassessed by apatite (U-Th)/He (AHe) thermochronology. In combination with available constraints on the orogenic structure, this new high resolution exhumation history sheds light on the mechanisms of "soft"-collision. These mechanisms are important in order to identify similarities and differences in collision mechanics between the East, SE and South Carpathians given for instance by the rheological properties of the lower orogenic plate, such as the contrast between the strong East

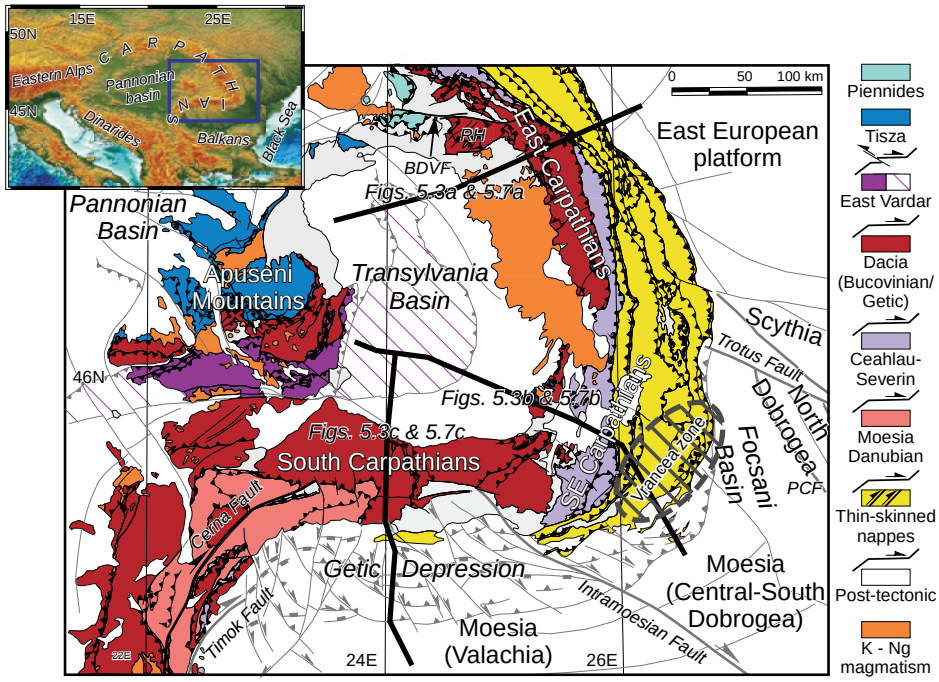

Figure 5.1: Tectonic map of the Romanian Carpathians with the locations of cross-sections in Figures 5.3 and 5.7 [simplified after *Matenco et al.*, 2007; *Schmid et al.*, 2008]. The upper left map shows the location in the Eastern Alps-Carpathians-Dinaridic system. The Vrancea zone marks the rough extent of the concentration of intermediate mantle earthquake-epicentres in the SE Carpathians. BDVF, Bogdan-Voda and Dragos-Voda fault systems; PCF, Peceneaga Camena Fault; RH, Rodna Horst.

European Platform vs. the weaker Moesian Platform [e.g. *Cloetingh et al.*, 2004] (Figure 5.1). The influence of such rheological contrasts during collisional exhumation of the upper orogenic plate and the thin-skinned wedge has not been addressed so far in thermochronological studies, although it is prone to induce large differences in vertical motions along the orogenic strike.

5.2 The Romanian Carpathians: framework of kinematics and collision

The Carpathians are the result of a Triassic to Tertiary evolution of continental blocks and intervening oceans. The continental blocks are Tisza-Dacia and ALCAPA located at the interior, and the European/Scythian/Moesian continental foreland along the exterior of the arcuate Romanian Carpathians (Figure 5.1) [e.g. *Csontos and Vörös*, 2004; *Schmid et al.*, 2008]. Two oceanic domains separated Tisza, Dacia and the foreland, namely the East Vardar Ocean to the west and the Ceahlău-Severin Ocean to the east (Figure 5.1). The East Vardar Ocean, part of the Neotethys, was situated between the Tisza and Dacia

continental blocks (Figure 5.1) and closed gradually during the Late Jurassic–Cretaceous. This closure was followed by continental collision during the late Early to Late Cretaceous [e.g. *Schmid et al.*, 2008]. The Ceahlău-Severin Ocean, part of the Alpine Tethys and of key importance for the Miocene Carpathian collision discussed in this study, opened between the Dacia block and the European/Scythian/Moesian foreland (Figure 5.1) during the Late Jurassic. It started to close during the late Early to Late Cretaceous. The Carpathian embayment, situated in a more eastward position in front of the Carpathians, did not close until the late Middle Miocene. This concave-shaped embayment follows the present-day curved configuration of the Carpathians and it was invaded by the Tisza-Dacia block in an upper plate position during the Neogene retreat of a slab associated with the Alpine Tethys, i.e. by subduction roll-back [e.g. *Ustaszewski et al.*, 2008]. During this invasion, suturing between the ALCAPA and Tisza-Dacia blocks took place during early Miocene times in the internal part of the East Carpathians (near the Bogdan-Voda and Dragos-Voda faults (BDVF); Figure 5.1) [*Tischler et al.*, 2007]. At the exterior of the Carpathians, all the relics of the Alpine Tethyan slab were entirely subducted at the time of termination of nappe emplacement over the European/Scythian/Moesian foreland ceased at ∼11 Ma [*Matenco and Bertotti*, 2000].

The Miocene outward-vergent thrusting in the highly arcuate Carpathian orogen was coeval with extension and subsidence observed in the back-arc basin (the Pannonian and Transylvania basins; Figure 5.1), similar to observations from other areas of the Africa/Europe collision zone [*Faccenna et al.*, 2004]. The subsidence led to the deposition of thick Middle–Upper Miocene sediments (up to 4 km) in the Transylvania Basin until ∼9 Ma, when the entire basin arrived at continental conditions. These Miocene sediments are not associated with large-scale normal faulting and massive lithospheric attenuation, as is the case in the Pannonian Basin [*Tari et al.*, 1992; *Dérerová et al.*, 2006]. The only significant structures at regional scale are shallow salt-decollements, which are accentuated near the East Carpathians due to an effect of loading and thermal sagging induced by the emplacement of overlying volcanic edifices [*Szakacs and Krézsek*, 2006].

Post-11 Ma crustal deformation peaked near the limit between Pliocene and Quaternary and was restricted to the area of the SE Carpathians (Figure 5.1; also see Chapter 4). A pronounced sea-level drop corresponding to the Messinian Salinity Crisis is recorded in the Carpathian foreland, and potentially enhanced erosional denudation around 5-6 Ma by increasing the exposure of source areas [*Leever et al.*, 2010]. Presently, strong mantle anisotropy characterises the Vrancea seismogenic zone of the SE Carpathians, with a high-velocity body observed in seismic tomography at depths of up to 370 km [*Martin et al.*, 2006]. This has been explained by a large number of often contradicting geodynamic models involving slabs or the evolution of continental blocks [see *Matenco et al.*, 2007 for a review]. The near-surface effects of the slab presently observed beneath Vrancea are generally interpreted as pull driving the ongoing subsidence observed in the SE Carpathian foreland [*Matenco et al.*, 2007].

5.3 Overview of thermochronology data of the East, SE and South Carpathians

A high-resolution exhumation history was derived for the SE Carpathians (Chapter 4). In order to integrate this into the general evolution of the Romanian Carpathians, additional data that constrain cooling through low temperatures were obtained by AHe dating of samples from the East and South Carpathians previously dated for AFT [*Sanders*, 1998; *Sanders et al.*, 1999]. See Chapter 2 and Appendix B (Tables B.5, B.6 and B.7) for a full overview of AHe analytical methods and data. The data set is further complemented by AFT and AHe data of *Sanders* [1998], *Schmid et al.* [1998], *Fügenschuh and Schmid* [2005], *Moser et al.* [2005], *Gröger* [2006], *Gröger et al.* [2008] and *Necea* [2010].

5.3.1 AHe thermochronology results

In the East Carpathians, vertical movements were traced along a ∼130 km long WSW-ENE trending profile with an average sample elevation of 707 ± 215 m (Figures 5.2 and 5.3a, Table 5.1). The transect crosses the folded sediments of the Transylvania Basin of Paleogene to Miocene in age, the Bucovinian crystalline basement, the Ceahlău unit and the Miocene external thrust belt (Figures 5.2 and 5.3a, Table 5.1). AHe ages of the six samples reassessed for AHe thermochronology range between 14 ± 1 Ma and 32 ± 5 Ma (Figures 5.2 and 5.3a, Tables 5.1 and B.5). AHe age replicates reproduce within uncertainty for most samples, with the exception of sample Carp 60 (Table B.5). The high age dispersion of this sample can likely be attributed to the low ^{238}U contents, and poor apatite quality, which makes the detection of inclusions more difficult, and therefore this sample is excluded for further geological interpretation (see Chapter 2 and Table B.5).

One sample from the East/SE Carpathians transition zone (Carp 69) was reassessed by AHe thermochronology to study the lateral change in exhumation histories between the East (Figure 5.3a) and SE Carpathians (Figure 5.3b). This sample yields an AHe age of 5.7 ± 0.5 Ma (Figure 5.2, Tables 5.1 and B.6).

In the South Carpathians, one of the 9 samples measured for AFT by *Sanders* [1998] from the Nehoiu Pass (Carp 36) was reassessed by AHe, yielding a much older AHe age of 63 ± 3 Ma (Figure 5.2, Tables 5.2 and B.7).

5.3.2 Discussion of AHe and AFT data

In the following sections, the new AHe results are integrated with previous thermochronology data of the East, SE and South Carpathians and will be discussed in more detail from NE to SW along the strike of the orogen (Figure 5.2). For comparison with the SE Carpathians (Chapter 4), samples are grouped in the following tectonic units: 1) Crystalline basement and Permo–Mesozoic cover of the Bucovinian/Getic nappes, 2) Mesozoic sediments of the Ceahlău-Severin unit, 3) Albian–Cenomanian post-tectonic cover, 4) Cretaceous–Paleogene turbidites of the Miocene external thrust belt, 5) Paleogene–Miocene hinterland sediments of the Transylvania Basin and 6) Post-collisional foredeep sediments (Figure 5.3, Tables 5.1 and 5.2).

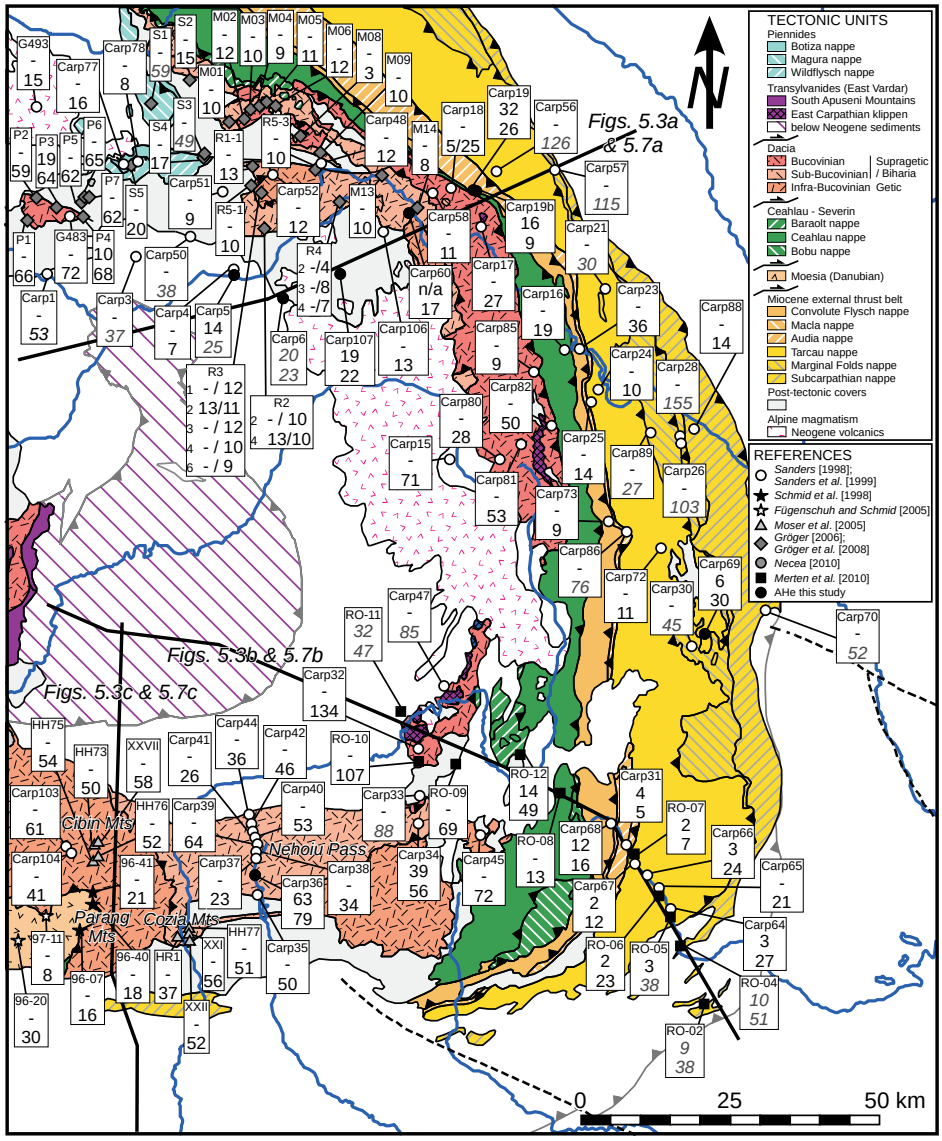

Figure 5.2: Simplified map of the East, SE and South Carpathians [after *Săndulescu*, 1984; *Visarion et al.*, 1988; *Matenco et al.*, 2003] depicting available and newly obtained low-temperature thermochronology data. Open circles, black stars, open stars, grey triangles, grey diamonds, grey circles, and black squares mark sample locations of *Sanders* [1998] and *Sanders et al.* [1999], *Schmid et al.* [1998], *Fügenschuh and Schmid* [2005], *Moser et al.* [2005], *Gröger* [2006] and *Gröger et al.* [2008], *Necea* [2010], and this study, respectively. Numbers in boxes from top to bottom represent sample code, AHe age and AFT age, respectively. Samples R2, R3 and R4 of *Gröger* [2006] and *Gröger et al.* [2008] represent vertical profiles with ages listed from high to low elevation. Depicted AHe ages are the error weighted averages of the α-corrected single grain ages. AFT ages are central ages, except for samples from *Moser et al.* [2005] and *Necea* [2010], who reported pooled ages for samples that passed the χ^2-test and central ages for samples with a P(χ^2) value <5%. Ages in grey italics represent non-reset ages (i.e. provenance ages). Solid black lines indicate locations of cross-sections in Figures 5.3 and 5.7.

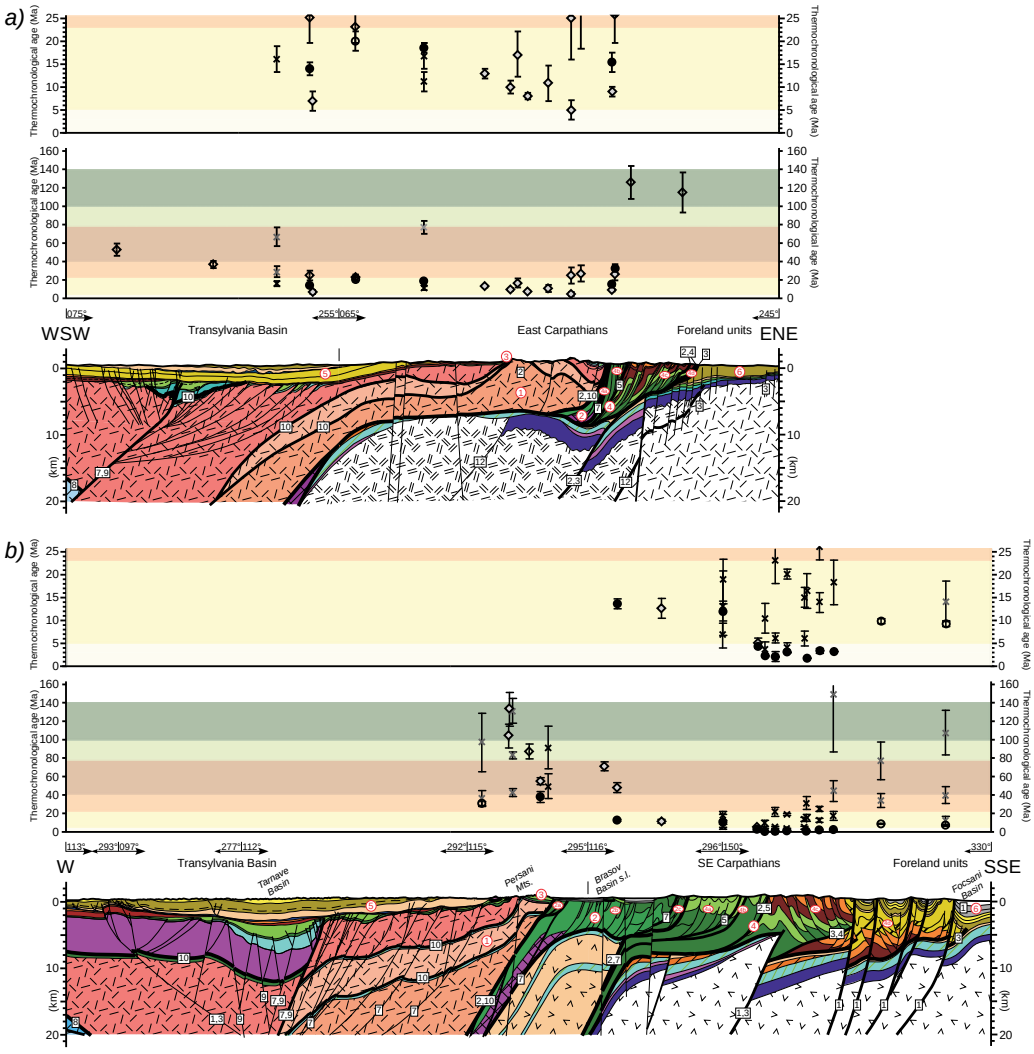

Figure 5.3: Geological cross-sections (2× vertical exaggeration) and thermochronological ages along three representative cross-sections in the Romanian Carpathians (location of cross-sections is depicted in Figures 5.1 and 5.2). Timing of deformation is taken from *Schmid et al.* [2008] and *Matenco et al.* [2010]. The interpretation of the Transylvania Basin is taken from depth-converted interpreted seismic lines calibrated by wells published by *Krézsek and Bally* [2006], *Szakács and Krézsek* [2006] and *Krézsek et al.* [2010]. The thermochronological plots on top of the cross-sections show AFT (diamonds and crosses, see legend) and AHe ages (circles, see legend). In Figures 5.3a and b, the lower thermochronological plots show the full age spectrum from 160 to 0 Ma and the top plots depict zoom-ins for 25 to 0 Ma). a) Regional section across the Transylvania Basin and the East Carpathians. The structure of the thin-skinned units and the foreland are controlled by seismic lines and wells [*Matenco and Bertotti*, 2000; *Tărăpoancă et al.*, 2003 and references therein]. The structure of the Bucovinian nappes and the underlying crustal structure are taken from surface geology, deep geophysical studies and regional interpretative cross-sections [*Ştefănescu et al.*, 1988b; *Kräutner and Bindea*, 2002]. Ages are from *Sanders* [1998], *Sanders et al.* [1999], *Gröger* [2006], *Gröger et al.* [2008] and this study. Strain partitioning near major strike-slips was excluded (e.g. BDVF; Figure 5.1).

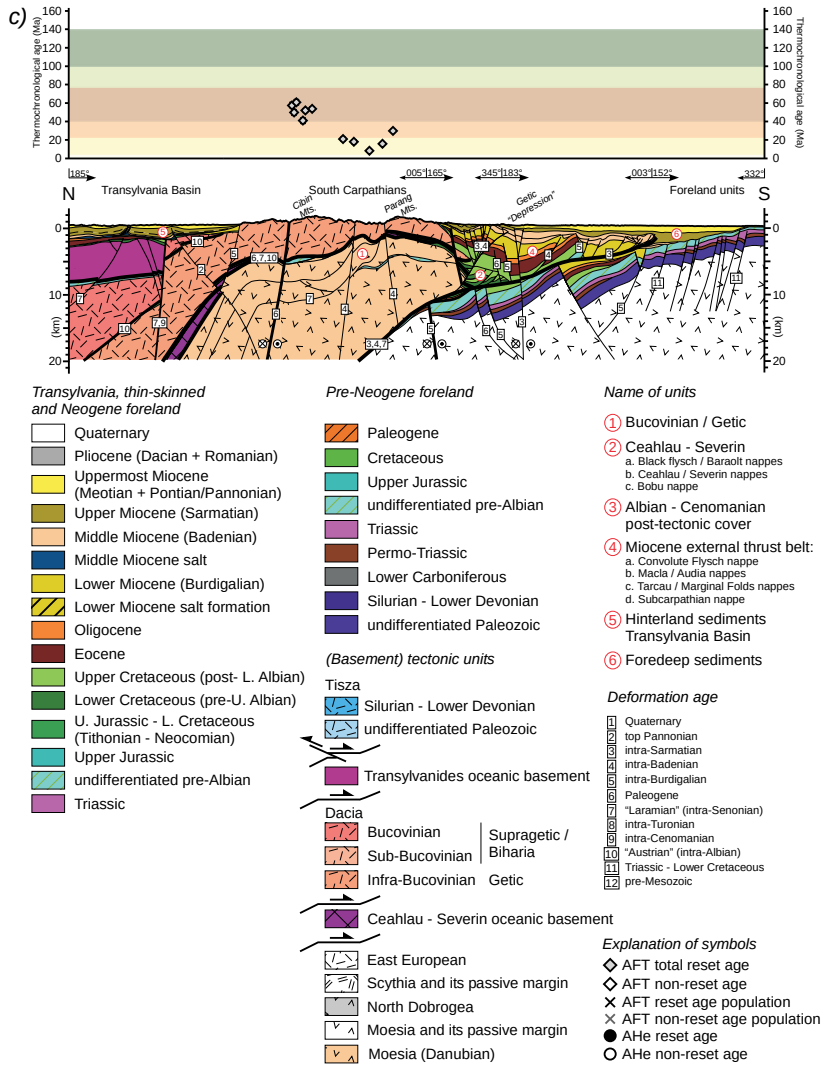

Figure 5.3: Continued. b) Regional section across the Transylvania Basin and the SE Carpathians after *Matenco et al.* [2007], *Schmid et al.* [2008] and this study (see chapter 4). Detailed interpretation based on seismic lines is available for the external thin-skinned nappes and the foreland [*Tărăpoancă et al.*, 2003; *Leever et al.*, 2006]. Ages are from *Sanders* [1998], *Sanders et al.* [1999] and this study. c) Regional section across the Transylvania Basin and the South Carpathians. The Getic Depression and the foreland units are well controlled by interpretation of seismic lines calibrated by wells [*Răbăgia and Matenco*, 1999; *Răbăgia et al.*, 2010; *Leever et al.*, 2010]. The interpretation of South Carpathian basement and its depth geometry are taken from lateral projection of surface studies [e.g. *Iancu et al.*, 2005 and references therein] calibrated by thermochronology [*Fügenschuh and Schmid*, 2005]. Another similarly interpreted cross-section, but located more to the west is available in *Schmid et al.* [2008]. Ages are from *Sanders* [1998], *Schmid et al.* [1998], *Fügenschuh and Schmid* [2005] and *Moser et al.* [2005].

The East and SE Carpathians

In the East Carpathians, AHe reset ages consistently are Oligocene–Miocene throughout the sample transect (Figures 5.2 and 5.3a, Table 5.1). Total or partial reset AFT ages of *Sanders et al.* [1999] and *Gröger* [2006] show a similar Oligocene–Miocene AFT age range for the Bucovinian basement, the internal nappes of the Miocene thrust belt and the Transylvania Basin sediments (Figures 5.2 and 5.3a, Table 5.1). Bucovinian basement samples dated by AFT [*Sanders*, 1998] (Carp 60, 58, 18 and 17) and *Gröger* [2006] (M13 and M14) all yield Miocene total reset central ages ranging between 5 ± 2 and 27 ± 9 Ma (Figures 5.2 and 5.3a, Table 5.1). In combination with the relatively long MTL of 13.4 ± 2.1 μm for sample M14 [*Gröger*, 2006], these AFT and AHe ages suggest rapid Miocene cooling of the Bucovinian basement in the East Carpathians. For the Miocene external thrust belt, two Lower Cretaceous samples from the Macla/Audia nappe yield total reset Oligocene–middle Miocene AHe and AFT ages (Figures 5.2 and 5.3a, Table 5.1). The AHe ages of 15 ± 2 Ma (Carp 19b) and 32 ± 5 Ma (Carp 19) are slightly older than or overlap the AFT ages of 9 ± 1 and 26 ± 6 Ma, respectively (Figures 5.2 and 5.3a, Table 5.1). However, incorporating the large error bars and the relatively long MTL of 13.5 ± 2.3 μm for sample Carp 19b [*Sanders*, 1998], on the overall thermochronology data suggest rapid Miocene cooling for the Macla/Audia nappe. For the Transylvania Basin, the Paleogene–middle Miocene sediments show a decrease in post-depositional thermal overprint from older to younger stratigraphic units (Table 5.1), as illustrated by a change from total reset AFT and AHe ages of 13 ± 1 to 22 ± 2 Ma for Eocene–Oligocene sediments (Carp 106 and 107) to non-reset AFT and AHe ages of 23 ± 3 and 20 ± 2 Ma for a Middle Miocene sediment sample (Carp 6). The latter was not buried deep enough to be reset prior to exhumation to the surface and records a provenance age. AFT data furthermore show an increase in thermal overprint from WSW to ENE by the change from non-reset ages of 53 ± 7 and 37 ± 4 Ma (Carp 1 and 3) to reset ages of 22 ± 2 and 7 ± 2 Ma (Carp 107 and 4), suggesting that the Transylvania Basin was exhumed more towards its margin at the contact with the East Carpathians (Figures 5.2 and 5.3a, Table 5.1). Samples from the more external Tarcău nappe are characterised by non-reset AFT ages of 126 ± 18 Ma (Carp 56) and 115 ± 22 Ma (Carp 57), suggesting that a significant early–middle Miocene thermal overprint is absent (Figures 5.2 and 5.3a, Table 5.1). Non-reset AFT ages suggest an Early Cretaceous provenance age for these Paleogene sediments from the Tarcău nappe.

In the SE Carpathian transect, reset AFT and AHe ages generally decrease from the internal Bucovinian basement nappes in the WNW to the Miocene external thin-skinned nappes in the SSE (Figures 5.2 and 5.3b, also see Chapter 4). Total or partial reset AFT ages range from 134 ± 18 Ma (Bucovinian basement) to 2 ± 1 Ma (Miocene external thrust belt). AHe ages are younger at 39 ± 6 Ma (Bucovinian basement) to 1.9 ± 0.1 Ma (Miocene external thrust belt). A similar pattern of overall decreasing reset AFT and AHe ages towards the foreland is indicated by the AFT and AHe data of *Necea* [2010] directly north of the transect (Figure 5.2).

The thermochronology data of the SE Carpathian transect show a much larger age spread compared to the East Carpathian transect, as illustrated by plots of

Table 5.1: Overview Sample Details and Thermochronological Data East Carpathians

Sample Details[a]						AHe[b]			AFT[c]						
Sample Code	Elevation (m)	Tectonic unit	Lithology	Stratigraphic age (Ma)		Age (Ma)	$N_{Repl.}$	$N_{av.}$	Age (Ma)	$P(\chi^2)$ %	Disp. (%)	$N_{Gr.}$	Pop. ages 1/2/3 (Ma)	MTL ± SD_L (µm)	N_L
East Carpathians															
Carp 1	450	5) Transylvanian hinterland	Sandstone	Oligocene-Miocene	33.9-5.8				*53 ± 7*	-	16	20		11.9 ± 1.4	45
Carp 3	500	5) Transylvanian hinterland	Sandstone	Miocene	23.8-5.8				*37 ± 4*	-	14	20		13.0 ± 1.4	21
Carp 50	600	5) Transylvanian hinterland	Sandstone	Lower Miocene	23.8-16.4				*38 ± 10*	-	67	72	16±3/29±6/67±10		
Carp 5	400	5) Transylvanian hinterland	Sandstone	Oligocene-Miocene	21.5-16.0	14 ± 1	3	2	*25 ± 5*	-	73	20			
Carp 4	400	5) Transylvanian hinterland	Sandstone	Oligocene-Miocene	21.5-16.0				7 ± 2	-	81	20		10.2 ± 2.3	6
Carp 6	600	5) Transylvanian hinterland	Dej tuff	Badenian	16.0-12.5	*20 ± 2*	4	4	*23 ± 3*	-	8	20		12.1 ± 0.9	13
Carp 107	1030	5) Transylvanian hinterland	Sandstone	Oligocene	28.4-23.8	19 ± 1	3	2	22 ± 2	-	78	86	11±2/17±3/77±7		
Carp 106	900	5) Transylvanian hinterland	Sandstone	Eocene - Oligocene	33.9-28.4				13 ± 1	-	26	48			
M13	930	1) Bucovinian nappe	-	-	-				10 ± 1	99	-	20			
Carp 60	830	1) Sub-Bucovinian nappe	Schist	-	-	n/a n/a	3	0	17 ± 5	-	89	46			
M14	850	1) Bucovinian nappe	-	-	-				8 ± 1	26	-	20		13.4 ± 2.1	43
Carp 58	770	1) Bucovinian nappe	Schist	-	-				11 ± 4	-	14	45			
Carp 18 (I)	1000	1) Bucovinian nappe	Quartzite	Lowermost Cretaceous	150.8-130.0				5 ± 2	-	14	27			
Carp 18 (II)	1000	1) Bucovinian nappe	Quartzite	Lowermost Cretaceous	150.8-130.0				25 ± 9	-	75	11			
Carp 17	800	1) Bucovinian nappe	Schist	-	-				27 ± 9	-	69	22			
Carp 19b	700	4) Audia nappe	Sandstone	Lower Cretaceous	145.5-99.6	15 ± 2	2	2	9 ± 1	-	14	42		13.5 ± 2.3	28
Carp 19	700	4) Audia nappe	Sandstone	Lower Cretaceous	145.5-99.7	32 ± 5	2	1	26 ± 6	-	77	19			
Carp 56	450	4) Tarcau nappe	Sandstone	Paleocene-Eocene	65.5-40.4				*126 ± 18*	-	49	18			
Carp 57	530	4) Tarcau nappe	Sandstone	Oligocene	37.2-23.0				*115 ± 22*	-	37	7			
Transition zone East / SE Carpathians															
Carp 69	370	4) Tarcau nappe	Sandstone	Paleocene - Eocene	65.5-40.4	5.7 ± 0.5	3	2	30 ± 8	-	52	77	11±1/30±5/41±17		

[a]Sample codes "Carp" are from the study of *Sanders* [1998]; "M" sample codes are from the study of *Gröger* [2006].

[b]Samples reassessed by AHe thermochronology in this study. Age is error weighted average of replicate AHe single grain ages ± 1σ standard error (Appendix B, Tables B.5 and B.6). Note that this error weighted average age has been used for further interpretation. Sample marked with n/a represents a sample for which average could not be calculated due to high dispersion in single grain ages and is omitted for further interpretation. Ages in italics represent non-reset ages; $N_{Repl.}$ is number of replicate single grain age measurements; $N_{Av.}$ is number of single grain ages taken into account for calculation of error weighted average age. See Chapter 2 and Tables B.5 and B.6 for details on AHe analytical methods and data.

[c]AFT results of *Sanders* [1998] and *Gröger* [2006]. Age is central age ± 1σ standard error [*Galbraith and Laslett*, 1993]; Ages in italics represent non-reset ages; $P(\chi^2)$ is probability obtaining Chi-square (χ^2) for n degrees of freedom (where n is number of crystals minus 1) [*Galbraith*, 1981; *Green*, 1981; *Brandon*, 1992]; Disp. is dispersion in single grain ages [*Galbraith and Laslett*, 1993]; $N_{Gr.}$ is number of dated apatite crystals; Pop. ages 1/2/3 are age components calculated by *Sanders* [1998]; MTL ± SD_L is mean track length ± standard deviation of track length distribution; N_L is number of horizontal confined tracks.

thermochronological ages versus depositional ages (Figure 5.4). Pre-Albian samples from the East Carpathians, including samples from the Bucovinian basement, consistently yield Oligocene–earliest Pliocene reset ages (5 ± 2 to 32 ± 5 Ma, Figure 5.4a). Pre-Albian samples from the SE Carpathians, however, yield a wide range of Cretaceous, Paleogene and Miocene reset age populations (Figure 5.4b). In the East Carpathians, post-Albian samples yield Miocene reset ages and Cretaceous, Paleogene and Miocene non-reset ages (Figure 5.4a). In the SE Carpathians, post-Albian samples yield reset and non-reset Cretaceous, Paleogene and Miocene age populations (Figure 5.4b). Furthermore, post-Albian samples from the SE Carpathians show a consistent Pliocene–Quaternary reset age population, which is not observed in the East Carpathians.

One lower Paleogene sandstone sample from the Tarcău nappe, located in the transition zone between the East and SE Carpathians, yields a reset AHe age of 6 ± 1 Ma (Carp 69; Figure 5.2 and Table 5.1). Similar latest Miocene–Pliocene total reset AFT and AHe ages are indicated for the Miocene external thrust belt in the SE Carpathians (e.g. Carp 31, Figure 5.2). The reset AFT age populations ranging between 11 ± 1 and 41 ± 17 Ma for Carp 69 [*Sanders et al.*, 1999] (Table 5.1) also correspond to the AFT ages of samples from the Tarcău nappe in the SE Carpathian transect (Figure 5.3b, also see Chapter 4). In this respect, sample Carp 69 from the transition zone between the East and SE Carpathians seems to be part of the SE Carpathian thermal evolution.

The South Carpathians

For the South Carpathians, one Supragetic basement sample from the Nehoiu Pass (Carp 36) yields an AHe age of 63 ± 3 Ma; *Sanders* [1998] obtained a latest Cretaceous AFT age of 79 ± 5 Ma (Figure 5.2 and Table 5.2). A plot of AFT ages versus elevation and MTLs of data from *Sanders* [1998] from the Nehoiu Pass (Figure 5.4a and Table 5.2), shows general latest Cretaceous–Oligocene ages. AFT ages overall decrease towards lower elevations, suggesting the onset of enhanced exhumation in Paleocene–Eocene times. Two AFT ages of samples close to the Moesian foreland (Carp 36 and 35; Figure 5.2) have latest Cretaceous–Paleocene AFT ages that are somewhat older with respect to sample elevation. Relatively long MTLs of 13.2 ± 1.3 μm (Carp 36) and 13.3 ± 1.7 μm (Carp 35) and the AFT/AHe age pairs (Carp 36) suggest a main latest Cretaceous–Paleocene cooling episode for these samples (Figure 5.5a and Table 5.2). Further to the west in the Cozia Mountains, AFT data of samples from the Supragetic nappe suggest Paleocene–Eocene cooling, as indicated by the decrease of AFT ages towards lower elevations (Figure 5.5a and Table 5.2) and thermal modelling [*Moser et al.*, 2005].

A transect through the Cibin and Parang Mountains shows a different AFT age distribution with younger ages towards the Moesian foreland (Figures 5.2 and 5.3c) [*Sanders*, 1998; *Schmid et al.*, 1998; *Fügenschuh and Schmid*, 2005; *Moser et al.*, 2005]. In the northern part of the transect (Figures 5.2 and 5.3c), ages in the Cibin Mountains range between 61 ± 3 (Carp 103) and 41 ± 3 Ma (Carp 104) and decrease towards lower elevations (Figure 5.5b and Table 5.2). In combination with relatively long MTLs of 12.2 ± 1.9 μm (Carp 104) to 14.0 ± 1.3 μm (HH75), this suggests latest Cretaceous–Eocene cooling (Figure 5.5b and Table 5.2). In the southern part of the transect (Figures 5.2 and 5.3c), AFT ages

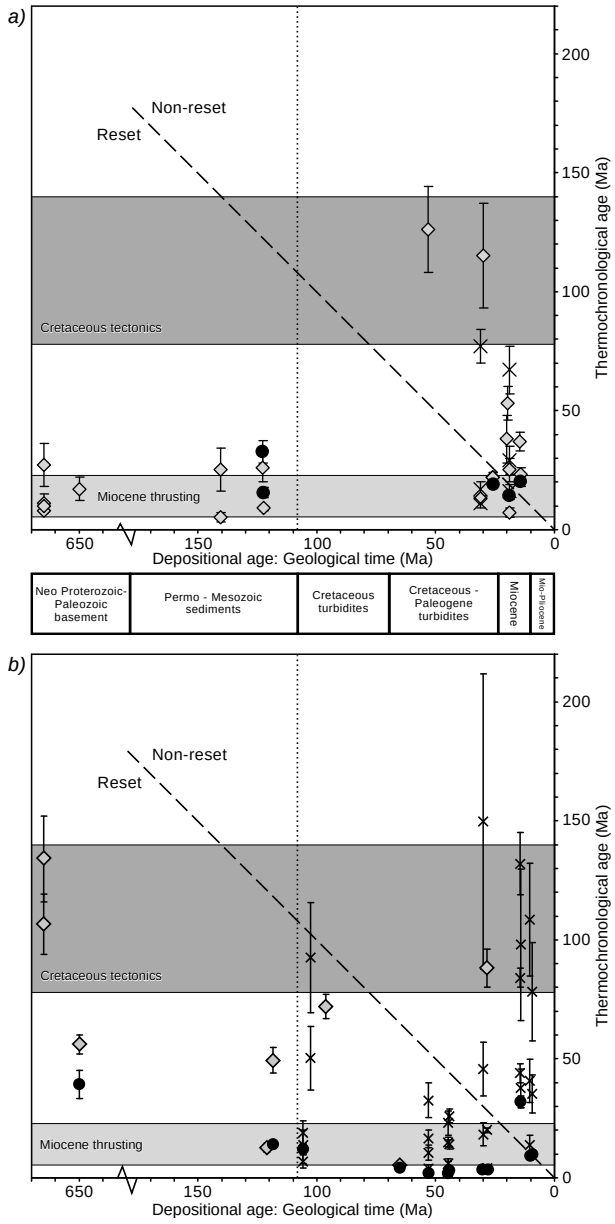

Figure 5.4: Thermochronological ages plotted against depositional age for a) the East Carpathian transect of Figure 5.3a, and for comparison b) the SE Carpathian transect (Figure 5.3b). Grey diamonds are AFT central ages and crosses are AFT age populations of *Sanders* [1998], *Sanders et al.* [1999], *Gröger* [2006], *Gröger et al.* [2008] and this study. Solid circles represent error weighted average AHe ages. Ages that fall below the dashed line are reset ages, and ages above the dashed line are not reset after deposition and give a provenance age. The dotted line marks the major Albian unconformity [e.g. *Ştefănescu*, 1976; *Kräutner*, 1980]. See text for further discussion.

Table 5.2: Overview Sample Details and Thermochronological Data South Carpathians

Sample Details					AHe[a]			AFT[b]						
Sample Code	**Reference**	**Elevation (m)**	**Tectonic unit**	**Lithology**	**Age ± 1σ (Ma)**	**$N_{Repl.}$**	**$N_{Av.}$**	**Age ± 1σ (Ma)**	**$P(\chi^2)$ %**	**Disp. (%)**	**$N_{Gr.}$**	**MTL ± SD_L (µm)**	**N_L**
Nehoiu Pass													
Carp 44	*Sanders* [1998]	900	1) Supragetic nappe	Schist				36 ± 4	-	15	41	10.0 ± 3.3	8
Carp 42	*Sanders* [1998]	1410	1) Supragetic nappe	Schist				46 ± 22	-	48	10		
Carp 41	*Sanders* [1998]	1580	1) Supragetic nappe	Schist				26 ± 7	-	27	32		
Carp 40	*Sanders* [1998]	1800	1) Supragetic nappe	Schist				53 ± 9	-	13	37		
Carp 39	*Sanders* [1998]	2050	1) Supragetic nappe	Schist				64 ± 10	-	13	35		
Carp 38	*Sanders* [1998]	1520	1) Supragetic nappe	Schist				34 ± 5	-	15	34	12.4 ± 1.9	44
Carp 37	*Sanders* [1998]	1220	1) Supragetic nappe	Schist				23 ± 8	-	15	27		
Carp 36	*Sanders* [1998]	1000	1) Supragetic nappe	Schist	63 ± 3	3	3	79 ± 5	-	11	30	13.2 ± 1.3	103
Carp 35	*Sanders* [1998]	870	1) Supragetic nappe	Schist				50 ± 4	-	10	24	13.3 ± 1.7	102
Cozia Mountains													
HH77	*Moser et al.* [2005]	1668	1) Supragetic nappe	Gneiss				*51 ± 3*	28	8	25	12.6 ± 1.8	45
XXI	*Moser et al.* [2005]	950	1) Supragetic nappe	Gneiss				*56 ± 3*	47	7	25		
XXII	*Moser et al.* [2005]	800	1) Supragetic nappe	Gneiss				*52 ± 3*	49	1	20		
HR1	*Moser et al.* [2005]	285	1) Supragetic nappe	Gneiss				*37 ± 2*	14	19	21		
Transect C-C'													
Cibin Mountains													
XXVII	*Moser et al.* [2005]	800	1) Getic nappe	Gneiss				*58 ± 3*	47	4	22	13.6 ± 1.2	19
HH73	*Moser et al.* [2005]	1195	1) Getic nappe	Gneiss				*50 ± 3*	96	0	26	13.8 ± 1.2	60
Carp 103	*Sanders* [1998]	2240	1) Getic nappe	Gneiss				61 ± 3	-	16	34	13.0 ± 1.6	60
Carp 104	*Sanders* [1998]	1200	1) Getic nappe	Gneiss				41 ± 3	-	11	37	12.2 ± 1.9	30
HH76	*Moser et al.* [2005]	1978	1) Getic nappe	Gneiss				52 ± 2	4	11	25	13.4 ± 1.2	50
HH75	*Moser et al.* [2005]	2100	1) Getic nappe	Gneiss				*54 ± 2*	26	6	20	14.0 ± 1.3	70
Parang Mountains													
96-41	*Schmid et al.* [1998]	750	1) Getic nappe	-				21 ± 2	91	-	19	12.9	65
96-40	*Schmid et al.* [1998]	1100	Danubian nappe	-				18 ± 2	96	-	19		
97-11	*Fügenschuh & Schmid* [2005]	1300	Danubian nappe	-				8 ± 1	64	-	11		
96-07	*Schmid et al.* [1998]	1900	Danubian nappe	-				16 ± 1	98	-	11		
96-20	*Fügenschuh & Schmid* [2005]	1150	Danubian nappe	-				30 ± 2	95	-	20	13.0 ± 1.8	100

[a]Sample reassessed by AHe thermochronology in this study. Age is error weighted average of replicate AHe single grain ages ± 1σ standard error (Appendix B, Table B.7). Note that this error weighted average age has been used for further interpretation; $N_{Repl.}$ is number of replicate single grain age measurements; $N_{Av.}$ is number of single grain ages taken into account for calculation of error weighted average age. See Chapter 2 and Table B.7 for details on AHe analytical methods and data.

[b]AFT results of *Sanders* [1998], *Moser et al.* [2005], *Schmid et al.* [1998] and *Fügenschuh & Schmid* [2005]. Age is central age ± 1σ standard error, except for ages in italics, which represent pooled ages [*Green*, 1981; *Galbraith and Laslett*, 1993]; $P(\chi^2)$ is probability obtaining Chi-square (χ^2) for n degrees of freedom (where n is number of crystals minus 1) [*Galbraith*, 1981; *Green*, 1981; *Brandon*, 1992]; Disp. is dispersion in single grain ages [*Galbraith and Laslett*, 1993]; $N_{Gr.}$ is number of dated apatite crystals; MTL ± SD_L is mean track length ± standard deviation of track length distribution; N_L is number of horizontal confined tracks.

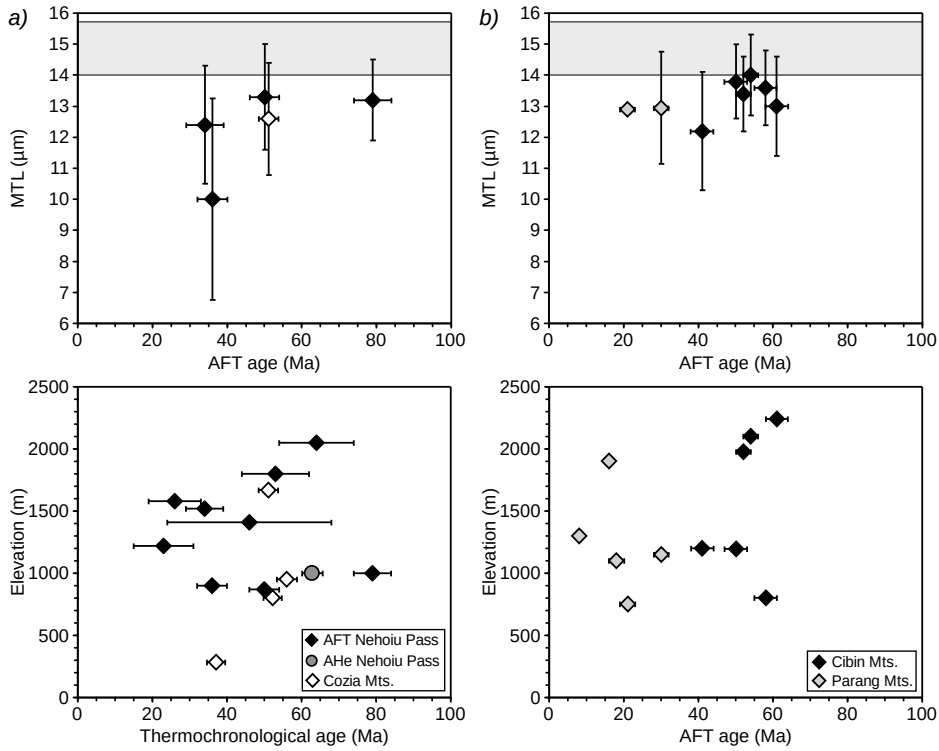

Figure 5.5: AFT age versus MTL plots (upper panels), and AFT age versus elevation plots (lower panels) for the crystalline basement of the South Carpathians. See Figure 5.2 for sample locations. Error bars on ages are ± 1s and MTL error bars are standard deviations of the track length distributions (Table 5.2). a) Thermochronology data for the Nehoiu Pass (black diamonds and grey circle) [*Sanders*, 1998; this study] and Cozia Mountains (open diamonds) [*Moser et al.*, 2005]. b) AFT data for the Cibin (black diamonds) [*Sanders*, 1998; *Moser et al.*, 2005] and Parang Mountains (grey diamonds) [*Schmid et al.*, 1998; *Fügenschuh and Schmid*, 2005].

in Parang Mountains are much younger than in the Cibin Mountains and range between 30 ± 2 Ma (sample 96-20) and 8 ± 1 Ma (sample 97-11). They show no consistent relation between age and elevation (Figure 5.5b and Table 5.2). MTLs of 12.9 (sample 96-41) to 13.0 ± 1.8 μm (sample 96-20) indicate some annealing (Figure 5.5b and Table 5.2). For this part of the transect through the Parang Mountains, AFT data suggest a Miocene cooling episode.

5.3.3 Time-temperature histories for the East, SE and South Carpathians

Time-temperature paths were modelled with the HeFTy program [*Ketcham*, 2005b], using AHe single grain ages integrated with AFT data of *Sanders* [1998] and geological constraints (e.g. stratigraphic unconformities and well constrained tectonic phases, Table 5.3). The present-day surface temperature was set to 10 ± 5°C.

For the East Carpathians, thermal models for Carp 19b, Carp 107 and Carp 5 suggest overall Oligocene–early Miocene burial, followed by rapid early–middle Miocene (∼17-12 Ma) cooling at rates of 13 ± 3°C/Ma (average of the samples ± standard deviation) and subsequent slow cooling at rates of 2.0 ± 0.2°C/Ma from the latest Miocene onwards (Figure 5.6a and Table 5.3). Oligocene sediments were buried to temperatures of ∼80-100°C (Carp 107), while younger Oligocene–Miocene sediments were buried to lower temperatures of ∼60-80°C (Carp 5) prior to early–middle Miocene cooling.

For the transition to the SE Carpathians, thermal modelling of Carp 69 was performed by incorporating constraints of the large-scale unconformity indicated by late Sarmatian sediments overlying the external part of the Tarcău nappe [e.g. *Murgeanu*, 1967]. The model suggests Eocene–early Miocene burial to temperatures of ∼100°C followed by a middle Miocene (∼13-11 Ma) cooling episode at ∼20°C/Ma (Figure 5.6b and Table 5.3). After late Miocene reburial to temperatures of ∼80°C, rapid cooling to surface temperatures at ∼34°C/Ma occurred between 6 and 4 Ma (Figure 5.6b and Table 5.3). Comparison of the modelled thermal history of Carp 69 with samples from the external SE Carpathians (Chapter 4) reveals that a similar time-temperature path with Paleogene burial, followed by middle Miocene cooling at rates of ∼19°C/Ma was obtained for RO-07 (Figure 5.6b and Chapter 4). Furthermore, latest Miocene-earliest Pliocene cooling at ∼33°C/Ma around 6-5 Ma was also indicated for Carp 31 (Figure 5.6b and Chapter 4). The cooling pulse around 3-1 Ma recorded by Carp 31 and RO-07 is not evident for Carp 69 (Figure 5.6b).

For the South Carpathians (Nehoiu Pass), thermal modelling of Carp 36 suggests latest Cretaceous–Paleocene cooling from >120°C to surface temperatures between 80 to 55 Ma at ∼5°C/Ma (Figure 5.6c and Table 5.3).

5.4 Exhumation and geometry during the Miocene collision of the Carpathians

The timing and onset of exhumation events suggested by the thermochronological data coincide with extensive deposition of clastic sediments both in the foreland (mainly thin-skinned turbiditic deposition) and in the hinterland (i.e. Transylvania basin) of the Carpathians. This suggests that Cretaceous–Quaternary cooling in the Carpathians can be ascribed to erosion resulting from either tectonic uplift or a base-level drop. Heating of rocks can generally be ascribed to burial by sedimentation. In order to derive post-Paleogene exhumation estimates (Table 5.3), regional heat flow data [*Veliciu and Visarion*, 1984; *Demetrescu et al.*, 2007] were used to calculate a constant (paleo)-geothermal gradient of 20 ± 5°C/Ma for the East Carpathians and 25 ± 10°C/Ma for the South Carpathians (see Chapter 2). This is in agreement with modelling results of the Miocene thermal evolution of the foreland basin [*Demetrescu et al.*, 2007].

On the overall, Miocene to present-day exhumation estimates (Figure 5.7) are in agreement with earlier low-temperature thermochronology studies, which demonstrated 4-6 km of Miocene–Quaternary bulk exhumation, erosional products distributed on both flanks of the Carpathian chain [*Sanders*, 1998; *Sanders et al.*, 1999; *Gröger*, 2006; *Gröger et al.*, 2008]. However, the new thermochronolog-

Table 5.3: HeFTty Modelling Constraints and Results

Sample details		Modelling constraints				No. paths[a]		AHe results[b]				Modelling results[c]					
Sample Code	Tectonic unit	Box	Constraint	Time (Ma)	Temp. (°C)	Acc.	Good	Grain	Mod. / Meas. AHe age (Ma)		GOF	Timing	C. rate (°C/Ma)	Ex. rate (mm/yr)	Error (+/-)	Ex./bur. (km)	Error (+/-)
East Carpathians																	
Carp 19b	4) Audia nappe	1	AFT age	18.3-8.0	120-80	4408	0	p1	16.6	/ 14.3	0.41	Early - Middle Miocene	14	0.7	0.2/0.1	4.3	1.4/0.9
	Lower Cretaceous	2	AHe age	18.0-7.8	85-40			p2	16.5	/ 20.1	0.41	Latest Miocene	2	0.1	0.0/0.0	1.0	0.3/0.2
Carp 107	5) Transylvania Basin	1	Stratigraphic age	28.4-23.8	20-5	3168	2395	p3	14.6	/ 14.6	1.00	Earliest Miocene	-12	-0.6	0.2/0.1	-4.0	1.3/0.8
	Oligocene	2	AFT age pop. 1 & 2	17.4-10.5	100-80							Early - Middle Miocene	15	0.8	0.3/0.2	2.7	0.9/0.5
		3	AHe age	16.0-10.5	85-40							Latest Miocene	2	0.1	0.0/0.0	1.4	0.5/0.3
Carp 5	5) Transylvania Basin	1	Stratigraphic age	21.5-16.0	20-5	931	628	p2	15.2	/ 15.3	0.86	Earliest Miocene	-22	-1.1	0.4/0.2	-2.8	0.9/0.6
	Oligocene-Miocene	2	AHe age	15.4-12.7	85-40			p3	15.2	/ 15.1	0.99	Early - Middle Miocene	10	0.5	0.2/0.1	1.5	0.5/0.3
												Latest Miocene	2	0.1	0.0/0.0	1.3	0.4/0.3
Transition zone East / SE Carpathians																	
Carp 69	4) Tarcau nappe	1	Stratigraphic age	65.5-40.4	20-5	2019	0	p2	5.7	/ 4.6	0.34	Paleogene	-4	-0.2	0.1/0.0	-4.8	1.6/1.0
	Paleocene-Eocene	2	AFT age pop. 2	35.0-25.0	120-100			p3	5.7	/ 6.3	0.35	Early - Middle Miocene	20	1.0	0.3/0.2	2.9	1.0/0.6
		3	AFT age pop. 1	12.0-10.0	100-80							Latest Miocene	-8	-0.4	0.1/0.1	-1.9	0.6/0.4
		4	Sarmatian unconformity	12.0-9.0	60-5							Pliocene	34	1.7	0.6/0.3	3.3	1.1/0.7
		5	AHe age	6.2-5.2	85-40							Quaternary	3	0.1	0.0/0.0	0.5	0.2/0.1
South Carpathians																	
Carp 36	1) Supragetic nappe	1	AFT age	84-74	120-80	25	0	p1	67.20	/ 59.10	0.06	Latest Cretaceous-	5	0.2	0.1/0.1	4.4	2.9/1.3
	crystalline basement	2	AHe age	66-60	85-40			p2	66.60	/ 67.30	0.87	Paleocene					
								p3	66.10	/ 80.50	0.06						

[a]No. paths, number of paths, where the total number of tried paths is 10,000; Acc., number of modelled acceptable paths (0.05<GOF<0.5, where GOF is the goodness of fit); Good, number of modelled good paths (GOF>0.5).

[b]Grain, AHe single grain ages taken into account for the model; Mod. He, modelled AHe single grain age; Meas. He, measured AHe single grain age; GOF, goodness of fit.

[c]C. rate, cooling rate (positive values represent cooling, negative values represent heating); Ex. rate, exhumation rate; Ex./bur., Estimated amounts of exhumation (positive values) or burial (negative values). Exhumation rates and estimates on the amount of exhumation and burial are calculated assuming a geothermal gradient of 20±5°C/km and 25±10°C/km for the East and South Carpathians respectively (see text and Chapter 2 for further details).

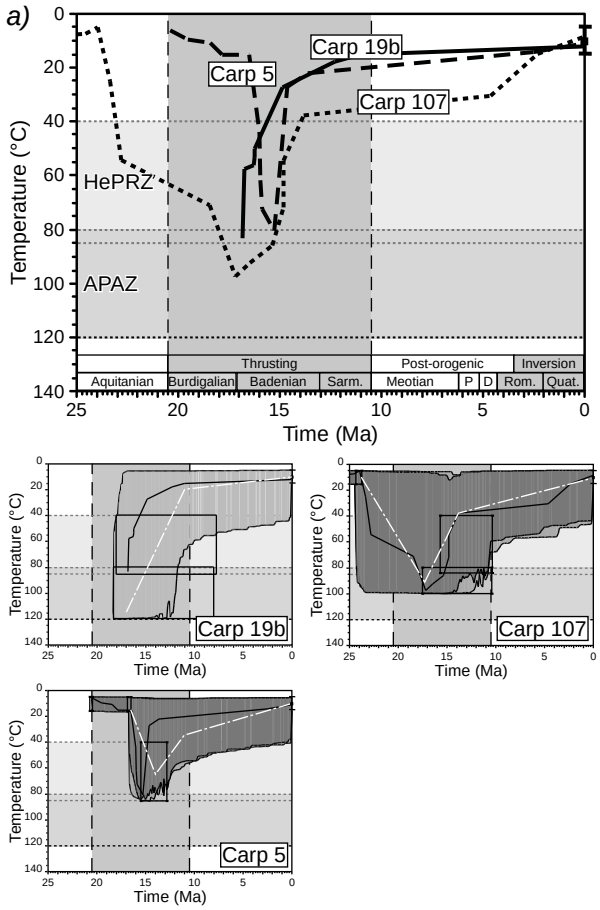

Figure 5.6: Thermal modelling results of AHe data (see Table 5.3 for an overview of modelling constraints and results). Present-day surface temperature is set to 10 ± 5°C. To allow a good comparison of modelling results per area, the best-fit time-temperature paths are depicted in the main graphs (left). The full modelled time-temperature histories including modelling constraints (black boxes), and good (dark grey) and acceptable (light grey) fit path envelopes are depicted in the smaller graphs (right). Numbers in boxes represent sample codes. In deriving cooling rates from the thermal histories, a smoothed version of the modelled best-fit thermal history was used (dashed white line). Based on the path envelopes, the uncertainties on the cooling rates are estimated to range from 10–50%, depending on the sub-segment. In the discussion of the data, however, no individual sample uncertainties on cooling rates are reported. Stages and tectonic phases are depicted along the x-axis of the main graphs. Periods of increased modelled exhumation are highlighted in grey shades. a) East Carpathian transect (Carp 19b, Carp 107 and Carp 5). b) East/SE Carpathian transition zone (Carp 69, Carp 31 and RO-07). e) South Carpathians, Nehoiu Pass (Carp 36).

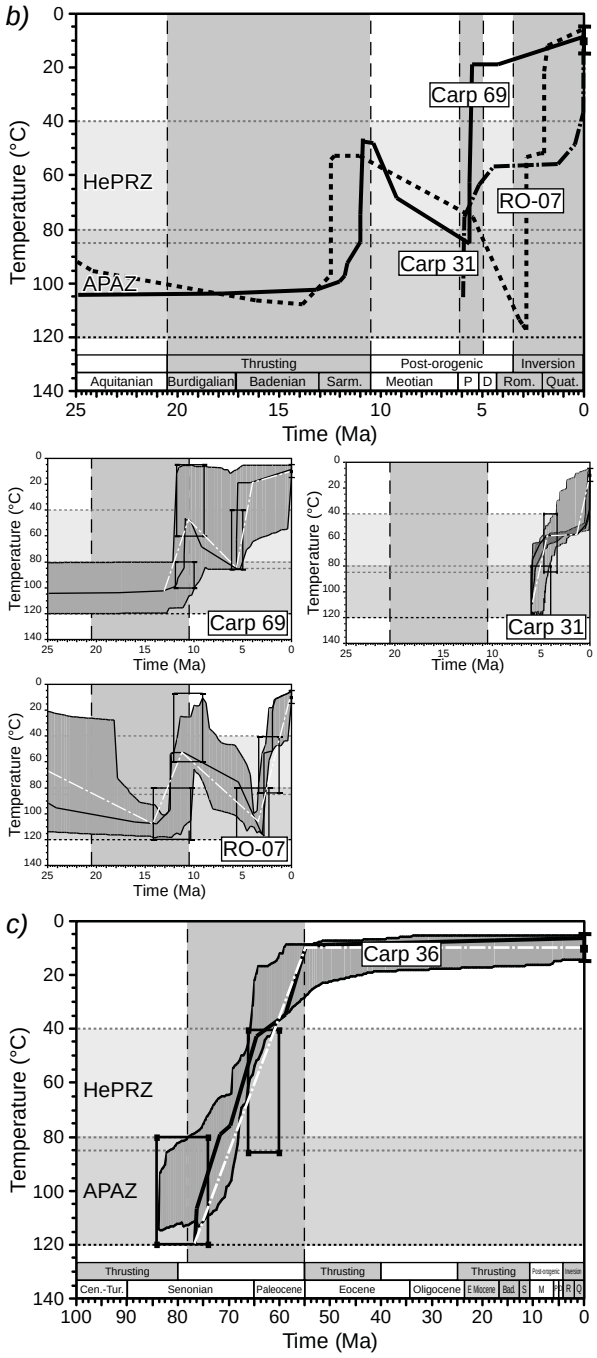

Figure 5.6: Continued

ical data are more discriminatory in terms of Miocene–Quaternary deformation episodes, as well as a separation between syn-collisional and post-collisional orogenic growth.

5.4.1 Miocene contraction and collision of the East and SE Carpathian nappes

The exhumation ages in the thin-skinned nappes of the East and SE Carpathians are generally middle–late Miocene, coinciding with the moment of their overthrusting over the thick continental European margin (Figures 5.3a and b). Older early–middle Miocene ages are associated with individual nappe emplacements in the East and SE Carpathians, which are difficult to distinguish as individual events by thermochronology alone (Figures 5.3a and b).

The present-day geometry of the Ceahlău suture zone in the East Carpathians forms a large antiform beneath the Bucovinian basement (Figure 5.3a). This antiformal shape is the result of deformation along high-angle thrusts truncating the European/Scythian lower plate, located in the foreland of the Ceahlău-Severin subduction zone [see also *Ştefănescu et al.*, 1988b]. This late stage deformation ramps up into the frontal sole thrust, where it is recognized in a system of antiformal stacks and out-of-sequence thrusts (Figure 5.3a). Thermochronology data indicate that the upper orogenic plate (i.e. the Bucovinian system) and part of the external thrust belt have been exhumed during the Miocene subduction and collision, as indicated by total reset AFT and AHe ages (Figures 5.2 and 5.3a). Major exhumation of the East Carpathian upper plate (Figure 5.3a) is restricted to the 13–8 Ma interval. The centre of the outcropping basement indicates slightly younger exhumation ages (10–8 Ma) compared to its flanks, which demonstrates that uplift and erosion continued until ∼9 Ma when the Transylvania basin was exhumed (Figure 5.3a). Estimated amounts of Miocene uplift and erosion range from 1.5–2.7 km for the Transylvania Basin sediments (Carp 5 and 107, respectively) to ∼4.3 km for the Audia nappe (Carp 19b) and likely occurred at a rate of 0.7 ± 0.1 mm/yr (Figure 5.7a and Table 5.3). The most external part of the thin-skinned wedge has not been exhumed at AFT resolution and exhumation

Figure 5.7 ***(facing page)*****:** a-c) Simplified crustal-scale versions of the cross-sections in Figure 5.3 through the a) East, b) SE and c) South Carpathians with post-Paleogene exhumation/burial estimates plotted on top. The cross-section through the East Carpathians was built outside the transpressional area of the Bogdan-Voda Dragos-Voda faults to avoid the localised effect of strain partitioning (see text). Note that the cross-section through the South Carpathians is located where the highest amount of Miocene exhumation is recorded. Grey lines below the cross-sections represent the base of lithosphere [after *Dérerová et al.*, 2006; *Horváth et al.*, 2006]. Note that the crustal sections have the same horizontal and vertical scales, while the sub-crustal lithosphere is vertically exaggerated. For further lithospheric details and the geometry of the Vrancea slab see *Martin et al.* [2006] and *Matenco et al.* [2007]. Exhumation/burial estimates are split into two phases, being 1) Early–Middle Miocene, and 2) Latest Miocene–Quaternary, except for the SE Carpathians where phase 2 is further divided into 2a) Latest Miocene, 2b) Pliocene and 2c) Quaternary. d) Simplified cross-section in the Central Alps along profile NFP20 East [*Schmid et al.*, 1996], illustrative for retro-shear collision.

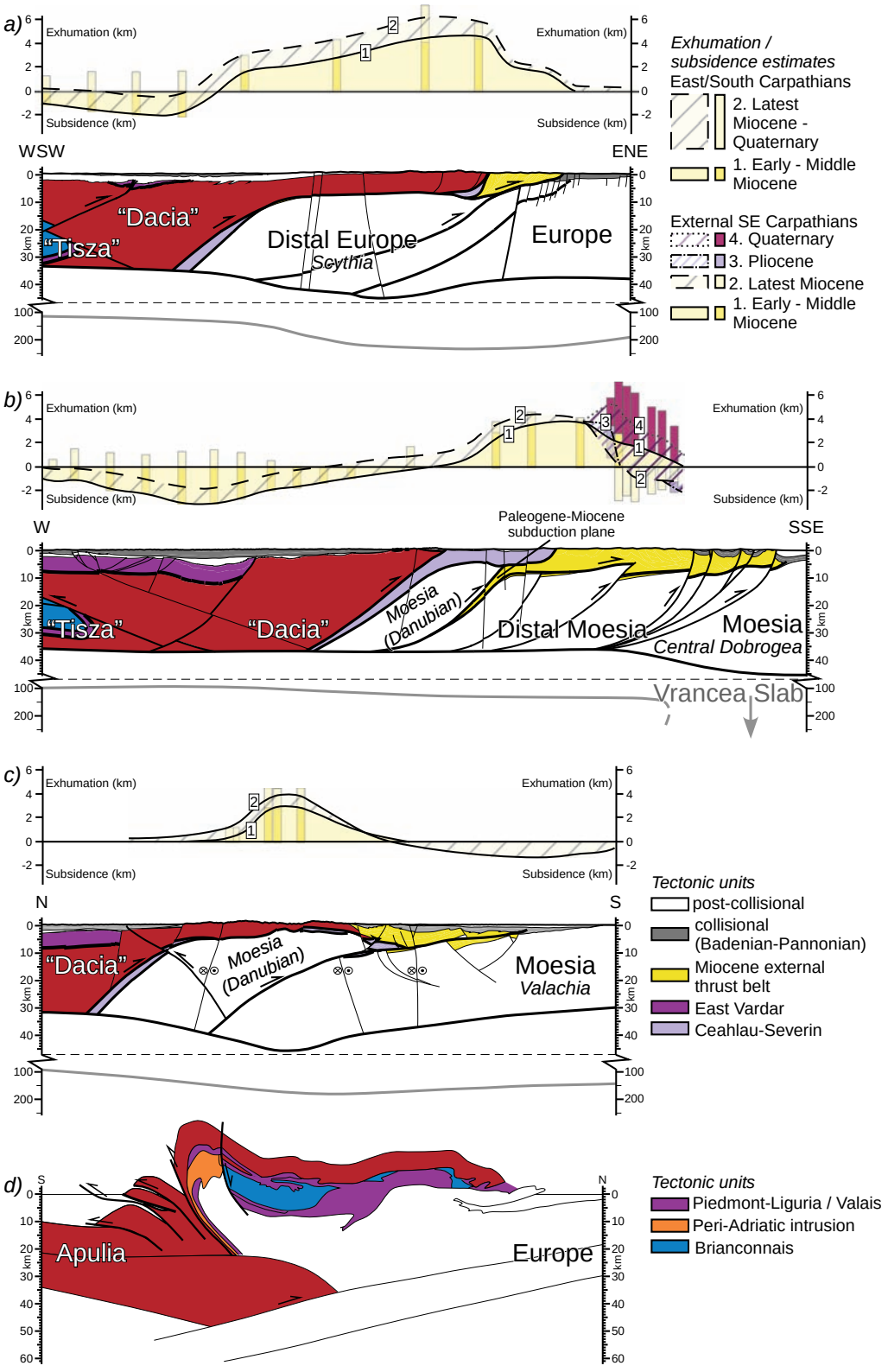
a)
Exhumation (km)
Subsidence (km)
WSW
ENE
"Dacia"
"Tisza"
Distal Europe
Scythia
Europe
Exhumation / subsidence estimates
East/South Carpathians
2. Latest Miocene - Quaternary
1. Early - Middle Miocene
External SE Carpathians
4. Quaternary
3. Pliocene
2. Latest Miocene
1. Early - Middle Miocene
b)
W
SSE
Paleogene-Miocene subduction plane
"Tisza"
"Dacia"
Moesia (Danubian)
Distal Moesia
Moesia
Central Dobrogea
Vrancea Slab
c)
N
S
"Dacia"
Moesia (Danubian)
Moesia
Valachia
Tectonic units
post-collisional
collisional (Badenian-Pannonian)
Miocene external thrust belt
East Vardar
Ceahlau-Severin
d)
Apulia
Europe
Tectonic units
Piedmont-Liguria / Valais
Peri-Adriatic intrusion
Brianconnais

estimates are in the order of <2 km (Figure 5.7a) [*Sanders et al.*, 1999]. The overall antiformal shape of exhumation can be correlated with the ramp anticline in the lower plate beneath the orogen (distal Europe in Figure 5.7a).

Significant Late Miocene (15–10 Ma) exhumation has been recorded by combined AFT and structural studies near the sinistral transcurrent system of the Bodgan-Voda Dragos-Voda faults (BDVF), located inside the Early Miocene suture between the internal ALCAPA and Tisza-Dacia blocks [*Sanders et al.*, 1999; *Tischler et al.*, 2007; *Gröger et al.*, 2008] (Figures 5.1). These studies indicated that strain partitioning at this major crustal boundary first led to folding and reverse faulting (16–12 Ma, AFT ages of 15–13 Ma), followed by fast exhumation of the Rodna horst during a second phase of tectonic activity (12–10 Ma, AFT ages of 13–8 Ma) along the BDVF (Figure 5.2) [*Tischler et al.*, 2007; *Gröger et al.*, 2008]. The sinistral transpression induced localised uplift [*Gröger et al.*, 2008], which added to the overall subduction and collisional exhumation (4–5 km) of the upper orogenic plate (Bucovinian nappes) and the internal part of the thin-skinned thrust belt. This is a local effect of strain partitioning along the inherited crustal boundaries in the upper plate basement and is, therefore, less relevant for the overall collision mechanics of the East Carpathians.

In contrast with the East Carpathians, the geometry of the SE Carpathians appears to show a much steeper contact between the upper plate Bucovinian basement and the Ceahlău-Severin subduction zone (Figure 5.3b). The Moesian lower plate and the sole thrust at the base of thin-skinned units are truncated by a number of younger high-angle thrusts. This depth geometry is indicated by seismic reflection/refraction studies and their derivatives in terms of tomographic inversion and ray-trace modelling [e.g. *Bocin et al.*, 2005; 2009; *Hauser et al.*, 2007]. In contrast with the East Carpathians, the basement of the SE Carpathians recorded only limited exhumation since the accretion of the Ceahlău-Severin nappe during Cretaceous times (Figures 5.3b and 5.7b). The Ceahlău unit and the Miocene external thrust belt do record significant Miocene exhumation (Figure 5.3b) with exhumation estimates in the order of 2–4 km at rates of ∼0.8 mm/yr (Figure 5.7b, Chapter 4). For the transition zone between the East and SE Carpathians, a similar amount of ∼2.9 km of Miocene exhumation at a rate of ∼1.0 mm/yr is estimated for the Miocene external thrust belt (Carp 69, Table 5.3). The exhumation pattern of the SE Carpathians (Figure 5.7b) cannot characterise an upper plate indentor during collision and suggests that continental units underlying the Ceahlău-Severin nappe (i.e. the Danubian nappes) are above the Paleogene–Miocene subduction zone of the Carpathian embayment (Figures 5.3b and 5.7b) [see also *Schmid et al.*, 2008]. This suggests that the Ceahlău-Severin subduction plane was abandoned and that the Paleogene–Miocene shortening of the SE part of the Carpathian embayment took mainly place on a subduction plane in front of the buried Danubian block, which was accreted to the upper plate at the end of Cretaceous times. This geometry is compatible with the South Carpathians, where Miocene thrusting takes place in the foreland of the exposed Danubian nappes, as demonstrated by outcrop studies (Figure 5.3c) [*Iancu et al.*, 2005].

5.4.2 Latest Miocene–Quaternary post-collisional exhumation of the East and SE Carpathians

The complete exhumation of the Transylvania Basin at ∼9 Ma [*Krézsek and Bally*, 2006] is coeval with the clustering of late Miocene exhumation ages (Figures 5.3a, b and 5.7a, b). Thermal models suggest continuous slow cooling for the East Carpathians following the late Sarmatian collision between Tisza-Dacia and the European/Scythian foreland (Figure 5.6a and Table 5.3). Exhumation estimates for the Transylvania Basin sediments and the East Carpathian nappes are 1.2 ± 0.2 km at a rate of ∼0.1 mm/yr (Figure 5.7a and Table 5.3). Latest Miocene–Quaternary exhumation estimates decrease to ∼0.5 km towards the foreland (Figure 5.7a).

The post-collisional evolution for the transition zone between the East and SE Carpathians shows a more complex exhumation history. Thermal modelling of Carp 69, located directly south of the Trotuş fault (Figure 5.2), suggests late Miocene reburial of ∼2 km at a rate of ∼0.4 mm/yr for the external Carpathian nappes (Figure 5.6b and Table 5.3). Late Miocene reburial is confirmed by the large-scale unconformity observed by late Sarmatian sediments overlying the external part of the Tarcău nappe [e.g. *Murgeanu*, 1967]. Exhumation in the order of ∼3.3 km resumed during the latest Miocene–early Pliocene at high rates of ∼1.7 mm/yr, followed by latest Pliocene–Pleistocene exhumation of ∼0.5 km at a rate of ∼0.1 mm/yr (Figure 5.6b and Table 5.3).

The post-collisional evolution of the external SE Carpathians shows a similar multi-phase exhumation history (also see Chapter 4). After the Sarmatian collision, the hinterland (Transylvania Basin, Bucovinian nappes and Ceahlău unit) was gradually uplifted and eroded (Figure 5.7b) at slow rates of ∼0.1 mm/yr (0.8 ± 0.4 km). The evolution of the SE Carpathian external thrust belt, however, was overprinted by two younger events indicated by exhumation ages clustering around two groups: at 5–6 Ma and at 2–3 Ma (Figures 5.3b and 5.7b, Chapter 4). After latest Miocene reburial of the external nappes coeval with rapid subsidence of the foredeep, the first post-collisional exhumation phase (Pliocene) in the central part of the Miocene external thrust belt (Figure 5.7b) occurred at high exhumation rates (∼1.7 mm/yr). This might be a tectonic event but is also coeval with the Messinian Salinity Crisis and with the desiccation of the Carpathian foreland basin due to the coeval Black Sea sea-level drop [*Gillet et al.*, 2007]. Because syn-tectonic patterns are absent in the nappes and foredeep sediments, this might be interpreted as climate-driven exhumation similar to a coeval event defined in the Alps [e.g. *Willett et al.*, 2006]. The second post-collisional exhumation phase suggests rapid Quaternary exhumation (3.8 ± 0.9 km at rates of 1.6 ± 0.3 mm/yr) for the external part of the Miocene thrust belt (Figure 5.7b). It is the result of the SE Carpathian inversion during the Quaternary, when high-angle reverse faults affected the lower plate and truncated the nappe pile with fold-like geometries near the surface (Figures 5.3b and 5.7b).

5.4.3 Exhumation history of the South Carpathians

The South Carpathian geometry is largely inherited from Cretaceous thick-skinned nappe emplacements, core-complex formation during latest Cretaceous–Eocene

orogen-parallel extension (i.e. the domal shape of the Danubian nappes) and dextral transtensional faulting during Oligocene–early Miocene times (Figure 5.3c) [*Răbăgia and Matenco*, 1999; *Fügenschuh and Schmid*, 2005; *Răbăgia et al.*, 2010]. These deformation phases correspond to the main pulses of exhumation recorded by a high-density distribution of zircon and apatite fission track ages, spanning the late Early Cretaceous to Paleogene [*Sanders*, 1998; *Bojar et al.*, 1998; *Schmid et al.*, 1998; *Willingshofer*, 2000; *Willingshofer et al.*, 2001; *Fügenschuh and Schmid*, 2005; *Moser et al.*, 2005]. In the South Carpathians, fission track data suggest a main latest Cretaceous–Eocene exhumation episode of ∼4.4 km at a time-integrated rate of ∼0.2 mm/yr (Figure 5.6c and Table 5.3). Additionally, heavy mineral spectra of Maastrichtian deposits in the South Carpathians suggest that the Getic nappe was the main source for Maastrichtian continental sedimentation. A change in heavy mineral content during the Maastrichtian suggests a latest Cretaceous onset of exhumation of the Danubian unit associated with updoming [*Bojar et al.*, 2010]. Latest Cretaceous–Paleogene exhumation might be related to the Paleogene–lower Miocene rotation of Tisza-Dacia around Moesia [senso *Ratschbacher et al.*, 1993] and more specifically to the latest Cretaceous–Eocene orogen parallel extension and exhumation of the Danubian units [*Fügenschuh and Schmid*, 2005].

Deformation associated with the Miocene collision is recorded by numerous faults in the Getic Depression, but the overall offset along the sole thrust is rather small when compared to the East or SE Carpathians (∼15-20 km in Figure 5.3c). The new AHe results for the South Carpathians suggest that no significant Miocene thermal overprint is recorded in the topographically highest area of the South Carpathians (Nehoiu Pass; Figure 5.2). This contradicts previous conclusions, which postulated that the South Carpathians experienced an exhumation episode related to the Miocene contractional processes in the external Carpathians [e.g. *Sanders*, 1998]. A small number of Miocene AFT ages have been obtained for the centre of the South Carpathians (Figures 5.2 and 5.3c) [*Schmid et al.*, 1998; *Fügenschuh and Schmid*, 2005] and the area to the SW, near the connection with the Dinarides [*Bojar et al.*, 1998] (Figure 5.1). One 8 Ma AFT age was measured in the centre of the exposed basement, the flanks were exhumed at best during the Middle Miocene shortening, samples having long residences in the partial annealing zone (Figure 5.3c). These exhumation ages have been interpreted as a result of the final stage of thrusting and transpression recorded by the thin-skinned units [*Fügenschuh and Schmid*, 2005]. Miocene thrusting took place beneath the Danubian nappes, i.e. far towards the foreland, indicating that the Ceahlău-Severin subduction zone was already locked (Figures 5.3c and 5.7c) [*Iancu et al.*, 2005].

5.5 Controls on the exhumation of the Romanian Carpathians and foreland-coupling collision

The geometry of the East, SE and South Carpathians is dominated by the asymmetry inherited from the late Early Cretaceous to Miocene period of subduction and continental collision between Tisza-Dacia and the European/Scythian/Moesian foreland. The timing of deformation is generally younger towards the foreland,

but out-of-sequence deformation is also observed and indicative for collisional stages (Figure 5.7).

The bulk exhumation recorded by low-temperature thermochronology in the East Carpathians is related to Miocene subduction and collision. Miocene exhumation ages are observed across the orogen, demonstrating that exhumation affected both the upper Tisza-Dacia plate and the thin-skinned nappes at the contact with the lower European/Scythian plate (Figure 5.7a). In the SE Carpathians, the Bucovinian basement recorded mainly Cretaceous–Paleogene exhumation events (Figure 5.2) and the Miocene exhumation is restricted to the Ceahlău unit and the external thrust belt (Figure 5.7b). These exhumation patterns change once more laterally in the South Carpathians where the restricted Miocene exhumation has locally preserved a topography resulting from Cretaceous–Paleogene pulses of orogenic building and core-complex formation, as demonstrated by exhumation ages (Figures 5.2 and 5.7c).

The entire studied area demonstrates the involvement of deep-seated basement thrusting affecting the lower orogenic plate into the collisional kinematics. This overall deformation of plate boundaries by gradual accretion of material from the lower plate during subduction and/or collision (Figure 5.8b) is rather a common process widely observed elsewhere [*Ziegler et al.*, 1995; *Roure*, 2008]. These duplications generate low amounts of exhumation that are detectable with low-temperature thermochronological studies. The new thermochronological data demonstrate that the foreland-coupling collision [*Matenco et al.*, 2010] is a viable mechanism for the Romanian Carpathians (Figure 5.8). The overall foreland-ward migration of exhumation (Figure 5.7) is diagnostic for this type of orogenic mechanics.

The exhumation histories and the interpreted vertical movements observed in the Carpathians also demonstrate significant differences along the orogenic strike. The two major units that compose the Carpathian lower plate (Europe/Scythia and Moesia; Figures 5.1 and 5.7) have a distinct strength contrast, which influences exhumation during collision [*Cloetingh et al.*, 2004]. In the mechanically strong European/Scythian domain, the Tisza-Dacia basement was stacked and exhumed together with the Ceahlău unit and the nappes of the external thrust belt during their Miocene emplacement (Figure 5.7a). The European/Scythian lower plate was deformed, but the major subduction boundary remained at the contact between Tisza-Dacia and the European/Scythian plate (i.e. the Ceahlău zone). This situation changes laterally in the SE and South Carpathians, where the upper Tisza-Dacia plate was accreted to the Danubian part of mechanically weaker Moesia (in the lower plate) at the end of the Cretaceous (Figures 5.7c and 5.8a). The SE Carpathians recorded further thrusting and duplications in the lower plate during Miocene–Quaternary times (Figure 5.8a).

The double-vergent orogens such as the Alps [*Schmid et al.*, 1996] exhume few tens of kilometres of material in the collision zone along retro-shears (Figure 5.7d). This type of accretion, although at far lower magnitudes, is also relevant for Carpathian-type orogens, which are dominated by subduction-related processes such as slab roll-back during separate episodes of thin-skinned nappe accretion. However, due to strong collisional coupling [senso *Ziegler et al.*, 1995], convergence can be accommodated by deformation along reverse faults inclined at a higher

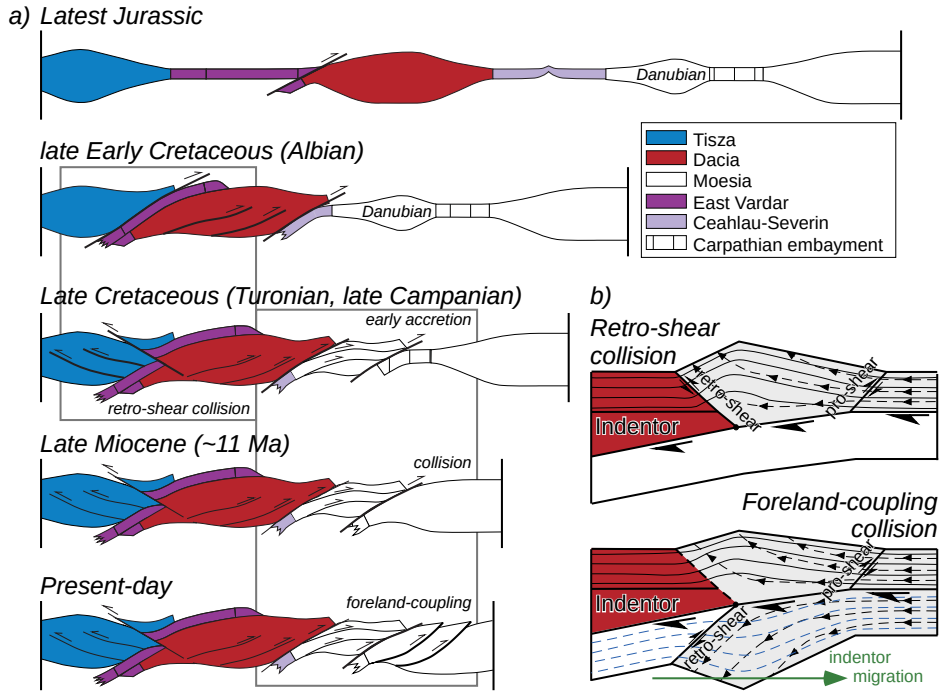

Figure 5.8: a) Sketch of plate-tectonic reconstruction along a transect crossing the SE Carpathians [modified after *Schmid et al.*, 2008]. b) Comparison between steady-state orogenic wedges starting from the mechanism of *Willett and Brandon* [2002] with particle paths and closure isotherms in the upper panel, as generic mechanism applicable for various high-convergence orogens. The equivalent foreland-coupling collision in the lower panel is a conceptual cartoon, i.e. not constrained by modelling. Blue dashed lines in the lower panel are strain lines.

angle than the subduction zone, particularly when thicker continental parts arrive at this zone (Figure 5.8a). These faults can be defined as retro-shears because the material entering the collision zone is moving towards the hinterland, but from a structural point of view these are foreland-vergent reverse faults. The foreland-coupling collision will distribute different exhumation ages across the orogen due to the gradual foreland-ward shift of accretion in the lower plate (Figure 5.8b). The latter is a deeper-seated mechanism and, therefore, the timing of activation can be detected by larger wavelengths of uplift near the surface and exhumation ages shifted towards the foreland. The orogens produced by foreland-coupling collision have a characteristic first order feature: crustal and lithospheric roots are not located beneath the core of the orogen, but shifted towards the foreland (Figures 5.7a-c).

The Romanian Carpathian scenario of subduction/collision is certainly not singular among Mediterranean-type orogens. Possible examples may include the buried "thrust-ridges" beneath the thin-skinned nappe pile of the West Carpathians (e.g. Silesian, Southern Magura) [*Poprawa and Malata*, 2006], which are foreland-coupling events in the lower plate (Paleozoic Europe) in respect to the

Pieniny Klippen Belt and Magura subduction zones [see also *Oszczypko*, 2006]. Cretaceous–Eocene deformations in the Dinarides (pre-dating the Miocene extension of the Pannonian basin) are almost exclusively concentrated in the lower plate, in respect to the Alpine Tethys (Sava) subduction zone. This is indicated by large-scale thrusting and exhumation recorded in the External Dinarides, East Bosnian-Durmitor, Drina-Ivanijca and Jadar-Kopaonik thick-skinned thrust sheets [e.g. *Schmid et al.*, 2008 and references therein]. Blind thrust faults with ramp-flat geometries of Quaternary age seem to be rooted at mid-crustal levels in the Adriatic lower plate beneath the Apennines. Here, deformation is observed near the surface through large areas of uplift with antiformal shape [*Picotti and Pazzaglia*, 2008]. Furthermore, basement thrusting post-dating nappe emplacement accounts for strain partitioning in the lower plate in many other orogens [*Roure*, 2008]. For example, the typical retro-shear collision in the European Alps also shows such potential foreland-coupling structures, such as localization of Pliocene deformation in the Paleozoic basins of the Jura Mountains beneath the intra-Triassic thin-skinned decollement [*Roure et al.*, 1994].

The foreland-coupling model of lower plate thickening is supported by a simple observation, confirmed by modelling studies: orogenic evolution is dependent on horizontal shortening, denudation and, last but not least, evolution of crustal roots [e.g. *Avouac and Burov*, 1996]. Numerical modelling suggests that it is easier to build crustal roots, shifted or not, than mountains at the topographic surface.